Binding of Cardiac Troponin-I$_{147-163}$ Induces a Structural Opening in Human Cardiac Troponin-C[†,‡]

Monica X. Li,[‡] Leo Spyracopoulos,[‡] and Brian D. Sykes*

MRC Group in Protein Structure and Function, Department of Biochemistry, University of Alberta, Edmonton, Alberta, Canada T6G 2H7

Received January 22, 1999; Revised Manuscript Received March 30, 1999

ABSTRACT: The interaction of troponin-C (TnC) with troponin-I (TnI) plays a central role in skeletal and cardiac muscle contraction. We have recently shown that the binding of Ca^{2+} to cardiac TnC (cTnC) does not induce an "opening" of the regulatory domain in order to interact with cTnI [Sia, S. K., et al. (1997) *J. Biol. Chem. 272*, 18216−18221; Spyracopoulos et al. (1997) *Biochemistry 36*, 12138−12146], which is in contrast to the regulatory N-domain of skeletal TnC (sTnC). This implies that the mode of interaction between cTnC and cTnI may be different than that between sTnC and sTnI. In sTnI, a region downstream from the inhibitory region (residues 115−131) has been shown to bind the exposed hydrophobic pocket of Ca^{2+}-saturated sNTnC [McKay, R. T., et al. (1997) *J. Biol. Chem. 272*, 28494−28500]. The present study demonstrates that the corresponding region in cTnI (residues 147−163) binds to the regulatory domain of cTnC only in the Ca^{2+}-saturated state to form a 1:1 complex, with an affinity approximately six times weaker than that between the skeletal counterparts. Thus, while Ca^{2+} does not cause opening, it is required for muscle regulation. The solution structure of the cNTnC·Ca^{2+}·cTnI$_{147-163}$ complex has been determined by multinuclear multidimensional NMR spectroscopy. The structure reveals an open conformation for cNTnC, similar to that of Ca^{2+}-saturated sNTnC. The bound peptide adopts a α-helical conformation spanning residues 150−157. The C-terminus of the peptide is unstructured. The open conformation for Ca^{2+}-saturated cNTnC in the presence of cTnI (residues 147−163) accommodates hydrophobic interactions between side chains of the peptide and side chains at the interface of A and B helices of cNTnC. Thus the mechanistic differences between the regulation of cardiac and skeletal muscle contraction can be understood in terms of different thermodynamics and kinetics equilibria between essentially the same structure states.

Ca^{2+}-dependent regulation of vertebrate skeletal and cardiac muscle contraction and relaxation is mediated by the troponin complex through interactions with tropomyosin and the actin filament. A succession of protein structural changes and altered protein−protein interactions are initiated by Ca^{2+} binding to the thin filament protein, troponin-C (TnC)[1]. The resultant signal is transmitted to the other members of the thin filament (troponin-I, troponin-T, tropomyosin, and actin), which in turn modifies the interaction between the thick and thin filaments, leading to muscle contraction [for reviews, see refs *1*−*4*]. Two isoforms of TnC exist in striated muscle, fast skeletal TnC (sTnC), and slow skeletal/cardiac TnC (cTnC). Both isoforms of TnC resemble a dumbbell with the N (regulatory) and C (structural) domains joined through a central linker. Each domain is comprised of two EF-hand helix-loop-helix motifs as potential Ca^{2+}-binding sites, except that site 1 in cTnC is inactive. While only site 2 in cTnC is required for triggering contraction in cardiac muscle, both sites 1 and 2 in sTnC are required for contraction in fast skeletal muscle (*5*, *6*).

Structural studies on sTnC (*7*−*12*) have demonstrated that Ca^{2+} binding to the N-domain induces a conformational transition from a "closed" to an "open" state. This transition involves large changes in interhelical angles with significant reorientation of helices B and C relative to the structural unit composed of helices N, A, and D. As a result, a hydrophobic patch on the surface of the molecule is exposed, which has been proposed to be the binding site for skeletal troponin-I (*13*). The analogous Ca^{2+}-induced change in the cardiac isoform was not known until we recently solved the solution structure of intact cTnC in Ca^{2+}-saturated state (*14*) and the structures of cNTnC in both the apo- and Ca^{2+}-saturated states (*15*). Strikingly, cNTnC remains essentially closed in the Ca^{2+}-saturated state, different from the open sNTnC·2Ca^{2+}. The significant reduction in the exposure of hydrophobic surface in Ca^{2+}-saturated cTnC compared to Ca^{2+}-saturated sTnC implies that the mode of interaction

[†] Supported by the Medical Research Council of Canada and the Heart and Stroke Foundation of Canada. L.S. is a Heart and Stroke Foundation of Canada Research Fellow.

[‡] The atomic coordinates for the final structures and the sets of restraints have been deposited with the RCSB protein data bank (accession code 1MXL).

* To whom correspondence should be addressed. E-mail: brian.sykes@ualberta.ca.

[‡] Both Authors contributed equally to this work.

[1] Abbreviations: TnC, troponin-C; sTnC, skeletal troponin-C; cTnC, cardiac troponin-C; cNTnC, N-domain (residues 1−89) of recombinant human cardiac troponin-C; sNTnC, N-domain (residues 1−90) of recombinant chicken skeletal troponin-C; sTnI, skeletal troponin-I; cTnI, cardiac troponin-I; cTnI$_{147-163}$, synthetic cardiac troponin-I peptide (residues 147−163); sTnI$_{115-131}$, synthetic skeletal troponin-I peptide (residues 115−131); NMR, nuclear magnetic resonance; HSQC, heteronuclear single-quantum coherence; NOE, nuclear Overhauser effect; rmsd, root-mean-square deviation; TFP, trifluoroperazine.

10.1021/bi9901679 CCC: $18.00
Published on Web 06/10/1999

between cardiac TnC and TnI may be different than that between skeletal TnC and TnI. In the simplest terms, for example, this raises the question of whether cTnC interacts with cTnI in a different manner than its skeletal counterparts, or whether the binding of cTnI is basically identical but the thermodynamics and the kinetics of the interaction are altered. In turn, these differences are reflected in the different physiological behavior of the two muscle types.

Structural information for TnI both in isolation and in complex with TnC/TnT is minimal. The NMR solution structure of sTnI inhibitory peptide while bound to sTnC determined by Campbell and Sykes (*16*) and the recently published crystal structure of the N-terminal sTnI fragment, residues 1−43, in complex with sTnC (*17*) are the only high-resolution structures available to date. Small-angle and neutron-scattering studies have proposed structure models for the sTnC·sTnI complex (*18*) and for sTnI and sTnC in situ within the ternary troponin complex (*19*). The interface between sTnI and sTnC has been shown to be in an antiparallel arrangement, involving multiple interaction sites between the two proteins [reviewed by Farah and Reinach (*3*); see also refs *20*−*22*].

Farah et al. (*23*) have suggested that residues 116−156 of sTnI are responsible for the expression of maximum inhibition, in addition to the inhibitory region (residues 105−115) (*24*). Van Eyk et al. (*25*) have reported that a TnI fragment encompassing only residues 96−148 is also able to elicit an inhibitory activity equivalent to that of intact TnI. Studies have also delineated the residues in the 96−148 region of TnI, which may interact directly with the N-domain of TnC. For example, Kobayashi et al. (*26*) have demonstrated that cysteine residues at positions 12 and 57 in the N-domain of sTnC can be cross-linked to sTnI regions 113−121 and 132−141, respectively. A recent fluorescence study by Pearlstone and Smillie (*27*) shows that within sTnI 96−148, residues 96−116 are primarily responsible for binding to the C-domain of TnC and residues 117−148 to the regulatory N-domain. Tripet et al. (*28*) have identified sTnI 115−131 ($sTnI_{115-131}$) as the region of TnI that directly interacts with the N-domain of TnC. We have monitored the titration of $sTnI_{115-131}$ to sNTnC·2Ca^{2+} using multinuclear, multidimensional NMR spectroscopy and demonstrated that it binds the hydrophobic pocket of sNTnC (*29*).

Little is known about regions of cTnI that are essential for the Ca^{2+} switch. However, an antiparallel arrangement between cTnC and cTnI has been proposed (*20*), an inhibitory region (residues 128−148 in human cTnI) has been identified (*24*), and cTnI 148−188 has been shown to be essential for the Ca^{2+}-dependent regulation of muscle activation (*30*). In this study, we focus on exploring the interaction between residues in the C-domain of cTnI and the N-domain of cTnC. On the basis of the sequence homology between sTnI and cTnI, residues 147−163 of cTnI, corresponding to residues 115−131 of sTnI, are the likely binding target for the regulatory domain of cTnC. In the present report, we examined the interaction between a synthetic cTnI fragment, $cTnI_{147-163}$, and cNTnC using multinuclear, multidimensional NMR spectroscopy. The data demonstrate that $cTnI_{147-163}$ binds to the N-domain of cTnC in the Ca^{2+}-saturated state with 1:1 stoichiometry. We have determined the three-dimensional solution structure of the complex of cNTnC·Ca^{2+} and $cTnI_{147-163}$. The most important finding is that $cTnI_{147-163}$ interacts with the hydrophobic core of cNTnC·Ca^{2+} and stabilizes the open conformation of cNTnC. The structure of the TnC-TnI complex has important implications for understanding the differences in regulation of cardiac and skeletal muscle contraction.

EXPERIMENTAL PROCEDURES

Construction of TnC Mutants, Protein Isolation, Peptide Synthesis, and NMR Sample Preparation. The engineering of the expression vector of cNTnC (1−89) mutant was as described in Chandra et al. (*31*). The expression of ^{15}N- and $^{15}N/^{13}C$-labeled protein in *Escherichia coli* was as described previously for sNTnC (*32*, *33*). Purification of the proteins followed the previously published procedure for cleaved TnC (*34*). Decalcification of ^{15}N-cNTnC and its NMR titration sample preparation was as described for ^{15}N-sNTnC (*33*). The synthetic peptide $cTnI_{147-163}$, acetyl-RISADAMM-QALLGARAK-amide, was prepared as described for $sTnI_{115-131}$ (*28*) and lyophilized twice to remove residual organic solvents. The sequence was confirmed by amino acid analysis, and the mass was verified by electrospray mass spectrometry. $cTnI_{147-163}$ peptides with specifically deuterated methyl groups were synthesized using corresponding deuterated amino acids from Cambridge Isotope Laboratories: *N-t*-BOC-L-leucine-d_{10} (D, 98%), *N-t*-BOC-L-alanine-3,3,3-d_3 (D, 98%), and L-methionine-methyl-d_3 (D, 98%). L-Methionine-methyl-d_3 (D, 98%) was N-terminally protected in-house. All NMR samples were 500 μL in volume. The buffer conditions were 100 mM KCl, 10 mM imidazole in 90% H_2O/10% D_2O, 15 mM dithiothreitol (DTT), and the pH was 6.8. For titration with peptide, 1.3 mL of ^{15}N-cNTnC was prepared and the concentration was determined to be 1.7 mM by amino acid analysis. The sample was divided into two equal portions: one sample contained 4 mM $CaCl_2$ (^{15}N-cNTnC·Ca^{2+}) and the other sample contained 5 mM EDTA (^{15}N-cNTnC·apo). For structure determination, NMR samples contained 1.5−3.0 mM protein, 6−8 mM Ca^{2+}, and 5.25−10.5 mM peptide.

$cTnI_{147-163}$ Titration of ^{15}N-cNTnC Monitored by 2D {^1H,^{15}N}-HSQC NMR Spectra. $cTnI_{147-163}$ is highly soluble in aqueous solution but tends to form a gel at high concentrations (>50 mM), likely due to aggregation. Thus, no stock peptide solution was prepared; instead, solid peptide was added at every titration point. The concentrations of ^{15}N-cNTnC and peptide were determined by amino acid analysis for every titration point, giving the $[cTnI_{147-163}]_{total}/[cNTnC]_{total}$ ratios. Both 1D ^1H and 2D {^1H,^{15}N}-HSQC NMR spectra were acquired at every titration point. Changes in pH associated with $cTnI_{147-163}$ additions were compensated by adjusting to pH 6.8 at every titration point. Two peptide titrations were performed, one using ^{15}N-cNTnC·apo and the other with ^{15}N-cNTnC·Ca^{2+}. The final $[cTnI_{147-163}]_{total}/[cNTnC]_{total}$ ratio was 3.5 in both cases.

NMR Spectroscopy. All of the NMR spectra were obtained using Unity INOVA 500 MHz or Unity 600 MHz spectrometers equipped with triple-resonance probes and *z*-axis actively shielded field gradients. All NMR spectra were acquired at 30 °C. Spectral processing and analyses were accomplished with the programs NMRPipe (*35*) and PIPP (*36*), respectively. 2D {^1H,^{15}N}-HSQC spectra were acquired using the sensitivity-enhanced gradient pulse scheme devel-

oped by Lewis E. Kay and co-workers (*37*, *38*). For cNTnC in the complex, sequential assignment of the backbone resonances was achieved using 3D ^{15}N-separated NOESY HSQC (150 ms) (*38*) and CBCA(CO)NNH experiments (*39*, *40*) in H_2O. Side-chain resonance assignments were accomplished with the HCCH-TOCSY experiment in H_2O (*41*, *42*). For $cTnI_{147-163}$ bound to ^{13}C,^{15}N-labeled cNTnC·Ca^{2+}, side-chain assignments for the peptide were accomplished using 2D ^{13}C/^{15}N F_1, F_2-filtered NOESY and 2D ^{13}C/^{15}N F_1-filtered DIPSI experiments in H_2O, which are modified versions of sequences proposed by Ogura et al. (*43*).

Structure Determination for cNTnC·Ca^{2+}·$cTnI_{147-163}$ Complex. Intramolecular distance restraints for cNTnC were obtained from ^{15}N-separated 3D NOESY HSQC NMR spectra (75 ms) (*38*) and simultaneous ^{15}N/^{13}C-separated 3D NOESY HSQC NMR spectra (75 ms) (*44*) in H_2O. Distance restraints for the 75 ms 3D NOESY HSQC experiments were calibrated as previously described (*45*), with the error on the peak intensities set to 40% and the lower bound on all proton−proton restraints set to 1.7 Å. Six distance restraints to the Ca^{2+} ion in site 2 were applied as previously described (*15*). The ϕ angle dihedral restraints were obtained from $^3J_{HNH\alpha}$ coupling constants derived from 3D HNHA NMR spectra acquired in H_2O (*46*). For the HNHA experiment, a correction factor of 1.055 was used, peak intensities were assumed to have errors of 25%, and the minimum restraint range was set to ±20°. The $d_{N\alpha}/d_{\alpha N}$ ratio was used to obtain loose dihedral restraints for the ψ angle of $-30° \pm 110°$ or $110° \pm 110°$, as reported previously (*32*). All valine and leucine methyl groups for cNTnC were stereospecifically assigned using 2D {^{1}H,^{13}C}-HSQC NMR spectra of a 30% ^{13}C-labeled sample (*47*). For bound $cTnI_{147-163}$, dihedral restraints of $-60° \pm 25°$ and $-30° \pm 25°$ for ϕ and ψ, respectively, were obtained from the chemical shift indices (CSI) of the peptide $^1H_\alpha$ protons for residues which showed α-helical CSI values. Intermolecular distance restraints for cNTnC methyl protons and $cTnI_{147-163}$ methyl protons were derived from 3D ^{13}C F_1-edited, F_3-filtered NOESY HSQC NMR spectra at mixing times of 75 ms, using a modified version of a pulse sequence reported by Ogura et al. (*43*). Additionally, 3D ^{13}C F_1-filtered, F_3-edited NOESY HSQC NMR spectra at mixing times of 75 ms employing linear frequency ramped broadband inversion pulses for ^{13}C were also acquired for detection of intermolecular NOEs in H_2O (*48*). Distance restraints from the intermolecular NOEs were set to 2 and 6 Å for the lower and upper limits, respectively.

Using an initial set of intramolecular NOE restraints for cNTnC·Ca^{2+}, 100 structures of cNTnC·Ca^{2+} without $cTnI_{147-163}$ were calculated starting from an extended conformation with the method of simulated annealing using the program XPLOR (*49*) with 50 ps of heating and 30 ps of cooling. Approximately 50% of the initial structures converged. Structure refinement was carried out with 30 converged structures with 50 ps of heating and 30 ps of cooling. ϕ, ψ dihedral angle restraints and seven distance restraints to Ca^{2+} in site 2 were added at later stages of the refinement processes. One hundred structures for cNTnC·Ca^{2+}·$cTnI_{147-163}$ were calculated starting from extended conformations for cNTnC and $cTnI_{147-163}$ with the simulated annealing protocol in XPLOR (*49*) using 65 ps of heating and 35 ps of cooling. Simulated annealing was carried out using the distance and dihedral restraints for cNTnC given in Table 1, seven distance to restraints to Ca^{2+} in site 2, 35 intermolecular distance restraints between protein and peptide methyls, 1 intermolecular distance restraint between the protein aromatic side chain of residue Phe-27 and peptide side chain methyls of residue Leu-157, and seven ϕ and eight ψ dihedral angle restraints, respectively, for $cTnI_{147-163}$. The final structures in the ensemble consisted of the 40 structures of lowest total energy from the initial family of 100 structures.

Table 1: Characteristics of the Solution Structure of cNTnC in the cNTnC·Ca^{2+}·$cTnI_{147-163}$ Complex

distance restraints	
total	1119
intraresidue	533
sequential ($\|i-j\|=1$)	246
medium ($2 \le \|i-j\| \le 4$)	212
long ($\|i-j\| \ge 5$)	128
dihedral restraints	48 ϕ, 49 ψ
restraints violation	
distance > 0.2 Å	23 (0.58/structure)
dihedral > 2°	0
rmsd (Å)[a]	
well-defined regions[b]	
Backbone atoms	0.67 ± 0.11
heavy atoms	1.14 ± 0.10
helix[c]	0.29
site 1 (res 29−40)	0.48 ± 0.12
site 2 (res 65−76)	0.32 ± 0.09
ϕ/ψ in most favored and additional allowed regions (all residues)[d]	97.4%

[a] Forty structures for cNTnC·Ca^{2+}·$cTnI_{147-163}$ were calculated using the simulated annealing protocol within XPLOR 3.1 (*49*). [b] Well-defined regions for cNTnC were residues 5−83. [c] The average of the N, A, B, C, and D backbone rmsds when each helix is separately superimposed to its average. [d] Backbone dihedral angle distributions were determined with the program PROCHECK (*53*).

RESULTS

$cTnI_{147-163}$ Titration of [^{15}N]-cNTnC·Ca^{2+}. Previously, we titrated Ca^{2+} into cNTnC and demonstrated that the addition of Ca^{2+} to cNTnC caused dramatic changes in the 2D {^{1}H,^{15}N}-HSQC NMR spectra (*50*). In this study, we show that additional chemical shift changes are induced by $cTnI_{147-163}$ binding to Ca^{2+}-saturated cNTnC. Figure 1A depicts the Ca^{2+}-induced shifts of backbone amide resonances in cNTnC. In comparison, Figure 1B depicts the $cTnI_{147-163}$-induced backbone amide resonance changes in cNTnC·Ca^{2+}. The 2D {^{1}H,^{15}N}-HSQC NMR spectra are completely assigned for cNTnC·apo, cNTnC·Ca^{2+}, and the cNTnC·Ca^{2+}·$cTnI_{147-163}$ complex, with the exception of the first two N-terminal residues and two prolines (Pro-52 and Pro-54). Most of the resonances fall into the fast exchange limit on the NMR time scale, except a few residues, which undergo large chemical shift changes: for example, Val-28, Glu-32, Ser-37, Gly-70, and Val-72 in Figure 1A and Val-28, Ser-37, Thr-38, and Val-64 in Figure 1B (*33*). The linear movement of cross-peaks in both titrations indicates single binding of Ca^{2+} to cNTnC and single binding of $cTnI_{147-163}$ to cNTnC·Ca^{2+}. Multiple binding of Ca^{2+} or peptide to cNTnC would lead to cross-peaks shifting in a nonlinear fashion in the 2D {^{1}H,^{15}N}-HSQC NMR spectrum, as observed in the case of TFP binding to cTnC (*51*). It is important to note that addition of $cTnI_{147-163}$ has negligible effect on the 2D {^{1}H,^{15}N}-HSQC NMR spectrum of cNTnC in the absence of Ca^{2+} (data not shown), indicating that Ca^{2+} is essential for cNTnC to interact with $cTnI_{147-163}$.

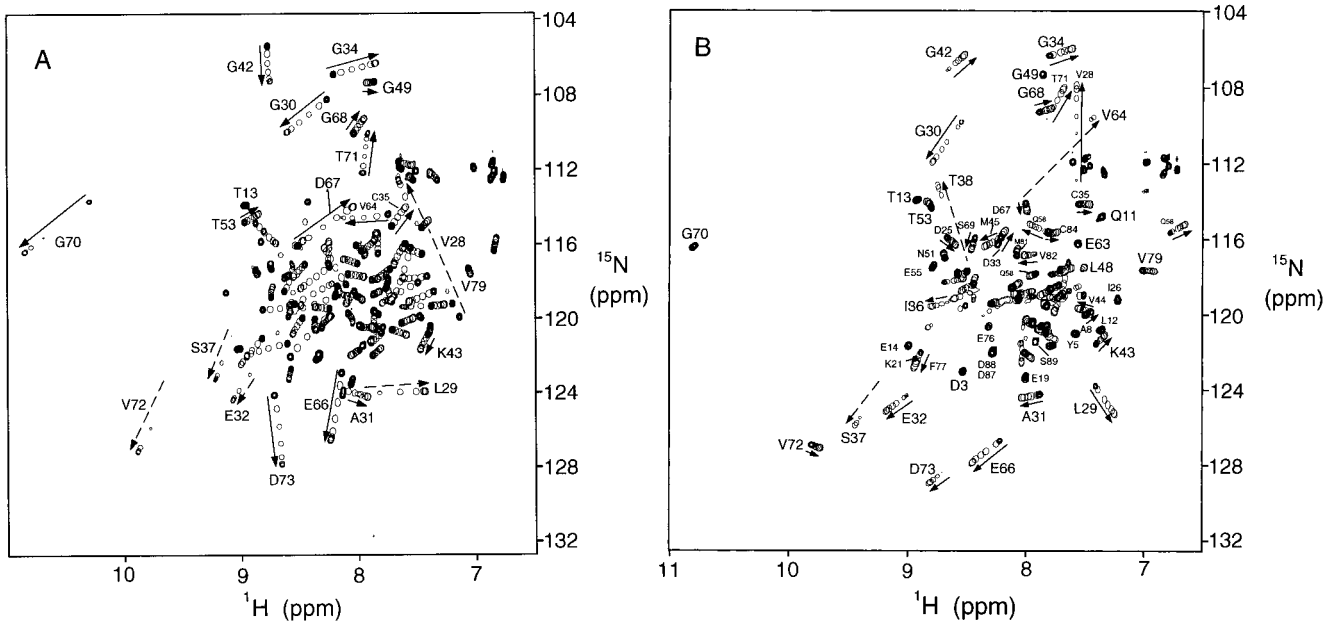

FIGURE 1: Titration of cNTnC·apo with Ca^{2+} (A) and cNTnC·Ca^{2+} with $cTnI_{147-163}$ (B). 2D {^{1}H,^{15}N}-HSQC NMR spectra from the backbone amide regions of cNTnC at various Ca^{2+} (A) and $cTnI_{147-163}$ (B) additions are superimposed, showing the progressive shift of peaks with increasing Ca^{2+} and $cTnI_{147-163}$ concentrations in panels A and B, respectively. Conditions are as described in Experimental Procedures.

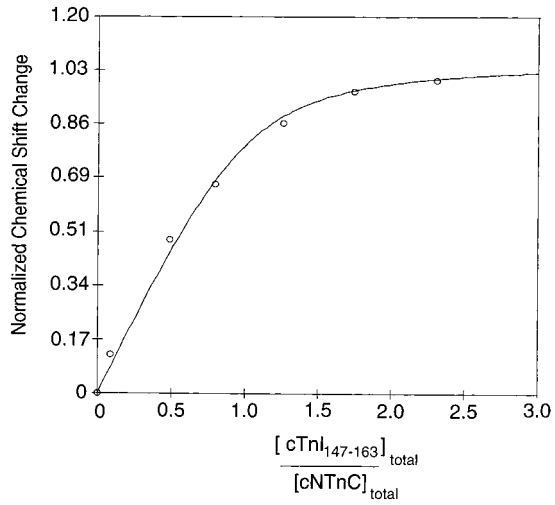

FIGURE 2: Titration of cNTnC·Ca^{2+} with $cTnI_{147-163}$. The curve represents the average of all residues followed in Figure 1B. The curve is normalized according to $(\delta_{obs} - \delta_{initial})/(\delta_{complex} - \delta_{initial})$. The best-fit curve to the data is shown by a solid line. Conditions are as described in Experimental Procedures.

Resonances of residues which show backbone amide ^1H_N and/or ^{15}N chemical shift changes during titration can be followed to monitor Ca^{2+} and $cTnI_{147-163}$ binding to cNTnC. Virtually all residues of cNTnC (except Met-1, Asp-2, Pro-52, and Pro-54) can be observed in the 2D {^{1}H,^{15}N}-HSQC NMR spectra, and all observed resonances (except Val-28, Ser-37, Thr-38, and Val-64) can be followed during the titrations with Ca^{2+} and $cTnI_{147-163}$. Plots of $cTnI_{147-163}$-induced chemical shift changes of individual amides of cNTnC·Ca^{2+} as a function of the $[cTnI_{147-163}]_{total}/[cNTnC\cdot Ca^{2+}]_{total}$ ratio gave similar curves, and the average curve for all amides is shown in Figure 2. In comparison to Ca^{2+} binding to cNTnC (*50*), for which the normalized average chemical shift change makes a sharp transition when the $[Ca^{2+}]_{total}/[cNTnC]_{total}$ ratio is 1, the normalized average chemical shift change upon $cTnI_{147-163}$ binding to cNTnC·Ca^{2+} does not level off so sharply at a $[cTnI_{147-163}]_{total}/[cNTnC\cdot Ca^{2+}]_{total}$ ratio of 1. This indicates that $cTnI_{147-163}$ binds cNTnC·Ca^{2+} with significantly weaker affinity than Ca^{2+} binding to cNTnC. The normalized average chemical shift data as a function of $[cTnI_{147-163}]_{total}/[cNTnC\cdot Ca^{2+}]_{total}$ for all amides were fit to the following equation (see McKay et al. (*29*) and references therein):

$$cNTnC\cdot Ca^{2+} + cTnI_{147-163} \rightleftharpoons cNTnC\cdot Ca^{2+}\cdot cTnI_{147-163}$$

and yielded a macroscopic dissociation constant (K_D) of 154 ± 10 μM, which is ~60 times greater than the dissociation constant of Ca^{2+} binding to cNTnC (*50*). This affinity is ~6 times weaker than $sTnI_{115-131}$ binding to sNTnC·$2Ca^{2+}$ (*29*).

To correlate the Ca^{2+} and $cTnI_{147-163}$-induced chemical shift changes of cNTnC to conformational changes in the protein, we plotted the chemical shift changes for backbone atoms against the protein sequence (Figure 3). Interestingly, most of the chemical shift perturbations induced by Ca^{2+} are located in the two Ca^{2+}-binding sites, whereas for $cTnI_{147-163}$ binding, residues at the beginning of the B-helix and at the end of the C-helix undergo significant chemical shift changes (Figure 3). For example, Asp-65, Asp-67, Gly-70, Thr-71, Val-72, and Asp-73 located in site 2 undergo large Ca^{2+}-induced chemical shift changes (Figure 3A) but small $cTnI_{147-163}$-induced changes (Figure 3B), while Glu-40 and Val-64 experience large $cTnI_{147-163}$-induced chemical shift changes (Figure 3B).

We have shown previously that the two hinges in the Ca^{2+}-induced structural opening of sNTnC reside primarily on residues Glu-41 (equivalent to Glu-40 in cTnC) and Val-65 (equivalent to Val-64 in cTnC) (*45*). The fact that $cTnI_{147-163}$ induces major chemical shift perturbations at the two hinge regions of cNTnC is consistent with a structural transition from a closed state to an open state. In addition, the chemical

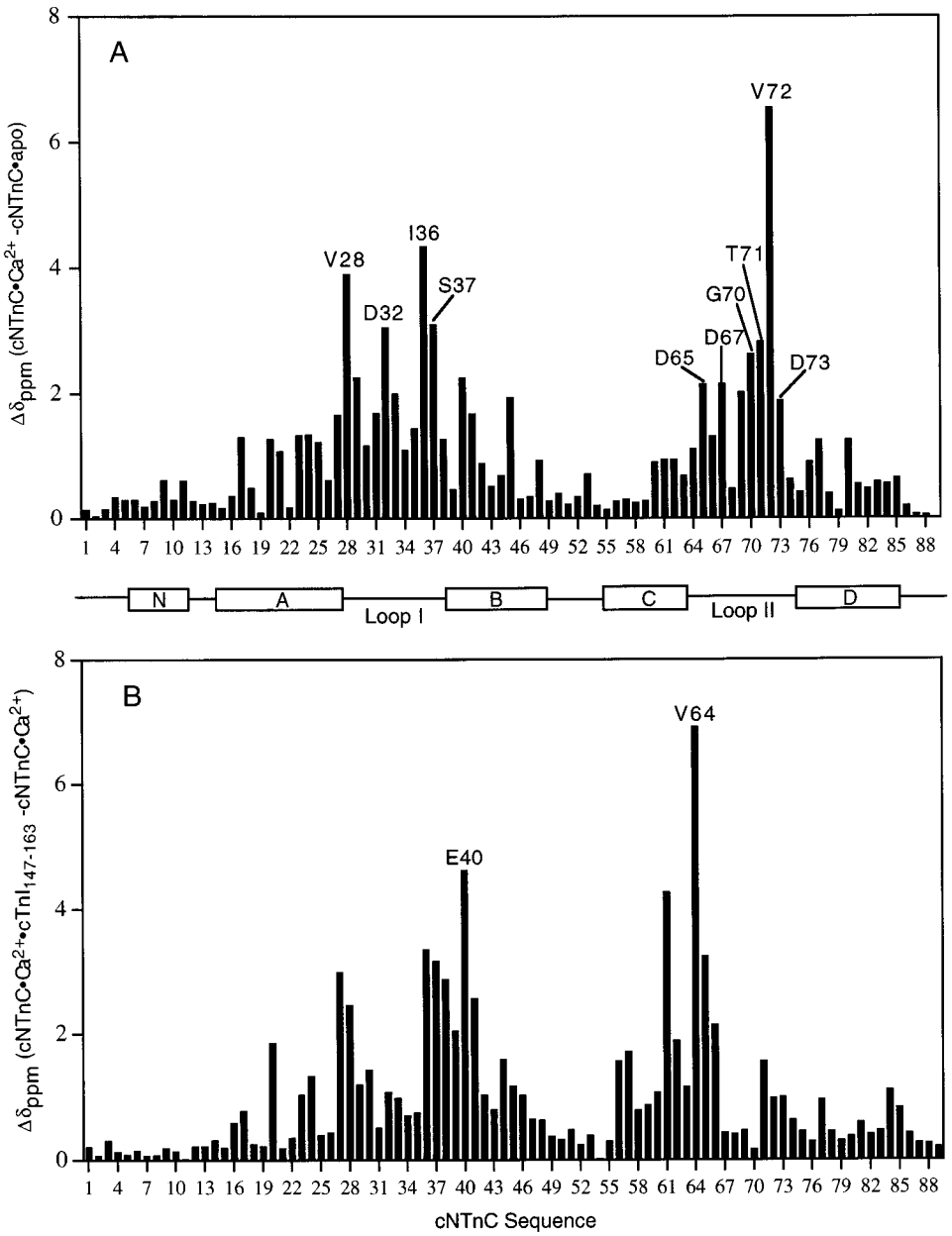

FIGURE 3: Comparison of Ca^{2+}-induced chemical shift changes for cNTnC·apo (A) and $cTnI_{147-163}$-induced chemical shift changes for cNTnC·Ca^{2+} (B). The chemical shift changes for each residue were calculated by averaging the normalized chemical shift change of the backbone $^1H_\alpha$, $^{13}C_\alpha$, ^1H_N, and ^{15}N chemical shifts. For a particular nucleus, the normalized chemical shift change of a residue is obtained by dividing the observed shift change by the average shift change for all residues. Thus, $\Delta\delta_{ppm} = 1$ indicates that the chemical shift change for a given residue is equal to the average change for all residues.

shift changes observed for the backbone amide of Val-64 as $cTnI_{147-163}$ binds to cNTnC·Ca^{2+} (Figure 1B) are similar to those observed for Val-65 in the apo (closed state) to Ca^{2+} (open state) transition for sNTnC (*32*). The backbone $^3J_{HNH\alpha}$ coupling constants for Glu-40 (5.9 Hz) and Val-64 (9.3 Hz) in the cNTnC·Ca^{2+}·$cTnI_{147-163}$ complex are closer to the ones observed for sNTnC in the Ca^{2+}-saturated state than to the ones expected for a closed structure (7.7 Hz for Glu-40 and 7.4 Hz for Val-64). These results indicate that the "kink" at Glu-40 observed in cNTnC·apo and cNTnC·Ca^{2+} (*15*) no longer exists and the ϕ dihedral angles for Glu-40 and Val-64 correspond to those for the open state.

Structure of cNTnC in the cNTnC·Ca^{2+}·$cTnI_{147-163}$ Complex. Overall structural statistics and conformational energies for the ensemble of solution structures are shown in Tables 1 and 2. The structures of cNTnC in the cNTnC·Ca^{2+}·$cTnI_{147-163}$ complex are of high quality, as indicated in Table 1 and Figure 4. The secondary structural elements of cNTnC in the cNTnC·Ca^{2+}·$cTnI_{147-163}$ complex are similar to those in cNTnC·apo and cNTnC·Ca^{2+} (*15*). The five helices, N, A, B, C, and D, are well-defined, superimposing with individual backbone rmsds of 0.21 ± 0.07 (N, residues 5−11), 0.35 ± 0.09 (A, residues 14−27), 0.21 ± 0.06 (B, residues 41−48), 0.29 ± 0.12 (C, residues 54−63), and 0.41 ± 0.09 Å (D, residues 74−83). Sites 1 and 2 are joined by a short twisted antiparallel β-sheet. The two Ca^{2+}-binding sites are nearly as well-defined as in the structure of cNTnC·Ca^{2+} (*15*) with backbone rmsd of about 0.5 Å. The β-sheet (residues 35−37, 71−73) is well-defined with a backbone rmsd of 0.21 ± 0.07 Å. The N- and C-terminal residues (residues 1−4 and 86−89) are less well defined than the helices and the β-sheet.

Table 2: Statistics of the Conformational Energies and rmsd for the Ensemble of Structures for cNTnC·Ca^{2+}·$cTnI_{147-163}$.

Energy (kcal mol^{-1})	
total	122 ± 2
bonds	2.2 ± 0.2
angles	97 ± 1
impropers	15.0 ± 0.3
van der Waals (F_{repel})[a]	3 ± 1
NOE restraints[b]	4 ± 1
dihedral restraints[b]	0.03 ± 0.03
rmsd from experimental restraints	
NOE distance restraints (Å)	0.008 ± 0.001
dihedral angle restraints (deg)	0.07 ± 0.03
rmsd from ideal covalent geometry	
bonds (Å)	0.00117 ± 0.00005
angles (deg)	0.465 ± 0.003
impropers	0.352 ± 0.003

[a] The force constant for the van der Waals energy (F_{repel}) calculation was 4.0 kcal mol^{-1} $Å^{-4}$. [b] Force constants for the calculation of NOE and dihedral energies were 50 and 200 kcal mol^{-1}, respectively.

The overall global fold of cNTnC in the cNTnC·Ca^{2+}·$cTnI_{147-163}$ complex is similar to the open sNTnC·$2Ca^{2+}$ structure as determined by solution NMR spectroscopy (*10*) and X-ray crystallography (*11*). The backbone atoms of the NAD unit of cNTnC in the cNTnC·Ca^{2+}·$cTnI_{147-163}$ complex superimpose onto the NAD unit of cNTnC·Ca^{2+} with an rmsd of 1.05 Å, indicating that binding of $cTnI_{147-163}$ does not induce a structural change in the NAD unit of cNTnC. This is not surprising, as the NAD unit is structurally invariant to Ca^{2+} binding in both c- and sNTnC. The BC unit, on the other hand, undergoes a large $cTnI_{147-163}$-induced structural change, as quantified by the interhelical angle changes in Table 3 and the exposure of a large hydrophobic patch which is involved in $cTnI_{147-163}$ binding (see below). The overall character of the $cTnI_{147-163}$-induced structural change in cNTnC in the cNTnC·Ca^{2+}·$cTnI_{147-163}$ complex is similar to the Ca^{2+}-induced structural transition in sNTnC (*10*).

Structure of $cTnI_{147-163}$ in the cNTnC·Ca^{2+}·$cTnI_{147-163}$ Complex. The 17 residue $cTnI_{147-163}$ peptide is expected to have high helix propensity, as determined by several secondary structural prediction protocols, which indicate that most of the peptide could likely adopt a helical conformation. The $^1H_\alpha$ NMR chemical shift index (*52*) at 5 °C for the peptide in H_2O indicates a helical region spanning residues 150−156. In the complex at 30 °C, the $^1H_\alpha$ chemical shift index also indicates a helical conformation spanning residues 150−156. In the ensemble of solution structures (Figure 4), $cTnI_{147-163}$ is α-helical from residues 151−156, and the backbone atoms of these residues superimpose onto the average peptide structure in the cNTnC·Ca^{2+}·$cTnI_{147-163}$ complex with a backbone rmsd of 0.32 ± 0.11 Å. The helical region and the N-terminus (residues 147−149) of the peptide interact with the protein, while the C-terminus (residues 157−163) does not interact with the protein and remains disordered in the ensemble of solution structures. The position of the N-terminal residues of $cTnI_{147-163}$ in the hydrophobic pocket of cNTnC in the complex is fairly well defined. The average rmsd for the backbone atoms of residues 150−156 of $cTnI_{147-163}$ is 1.03 Å when the backbone atoms of residues 5−83 of cNTnC in the ensemble of solution structures for the cNTnC·Ca^{2+}·$cTnI_{147-163}$ complex are superimposed onto the average cNTnC structure. In contrast, the average rmsd for the backbone atoms of residues 159−163 of $cTnI_{147-163}$ is 5.3 Å when the backbone atoms of residues 5−83 of cNTnC in the ensemble of solution structures for the cNTnC·Ca^{2+}·$cTnI_{147-163}$ complex are superimposed onto the average cNTnC structure. The stereochemical quality of the peptide structures in the ensemble of solution structures for cNTnC·Ca^{2+}·$cTnI_{147-163}$ is not as high-quality as the structures of cNTnC in the cNTnC·Ca^{2+}·$cTnI_{147-163}$ complex, as determined using the program PROCHECK (*53*). This is due in part to the lack of intramolecular NOEs for the peptide, the lack of stereospecific assignments for Leu-157 and Leu-158 in the peptide, and the fact that there are no experimental restraints of any kind for residues 159−163 of the peptide.

NOEs between cNTnC·Ca^{2+} and $cTnI_{147-163}$. Strip plots taken from the 3D ^{13}C F_1-edited, F_3-filtered NOESY−HSQC spectrum of the cNTnC·Ca^{2+}·$cTnI_{147-163}$ complex are shown in Figure 5A. In this spectrum, only NOEs arising from protein protons (attached to ^{13}C) and terminating on peptide protons (attached to ^{12}C) are observed. For example, the methyl groups of Ala-22 and Ala-23 in the A-helix of cNTnC and Met-45 and Met-47 located in the B-helix of cNTnC show strong NOE contacts with methyl groups of alanine, methionine, and leucine residues of unlabeled $cTnI_{147-163}$, indicating that the peptide interacts with the AB helical interface of cNTnC. These NOEs were also observed in the simultaneous 3D $^{13}C/^{15}N$-edited NOESY HSQC NMR spectrum of cNTnC in the complex, but no symmetrical peaks were present, indicating that they are intermolecular NOEs between cNTnC and $cTnI_{147-163}$. Interestingly, NOE connectivities observed between the A and B helices in the closed conformation of cNTnC·Ca^{2+} were not observed (*14*, *15*), which suggests that cNTnC in the complex is in an open conformation. The dissociation constant for $cTnI_{147-163}$ binding to cNTnC·Ca^{2+} of 154 μM indicates fast exchange between bound and unbound peptide. Thus, the chemical shifts for the peptide in the cNTnC·Ca^{2+}·$cTnI_{147-163}$ complex will be a weighted average between the two species. As the free peptide is unstructured at 30 °C, most of the methyl groups for particular residue types have degenerate or nearly degenerate chemical shifts. NOEs between peptide methyl groups with degenerate chemical shifts and cNTnC were unambiguously assigned by using two peptides which contained specifically deuterated methyl groups, except for leucine residues, for which all ^{12}C-bound ^1H were replaced with ^2H. One peptide (P1) contained deuterated methyl groups at Met-153, Ala-156, Leu-157, and Ala-160, and the other peptide (P2) contained deuterated methyl groups at residues Ala-150, Met-154, Leu-158, and Ala-162. Figure 5B demonstrates the utility of these two peptides in obtaining unambiguous intermolecular contacts for the cNTnC·Ca^{2+}·$cTnI_{147-163}$ complex. Figure 5C summarizes the residue pairs for which intermolecular NOEs between cNTnC and $cTnI_{147-163}$ are observed. Ala-150, Met-154, Leu-158, and Ala-162 are located on one side of the hydrophobic face of the peptide, and Met-153, Ala-156, Leu-157, and Ala-160 are located on the opposite side of the hydrophobic face of the peptide.

Structure of the cNTnC·Ca^{2+}·$cTnI_{147-163}$ Complex. As shown in Figure 6, $cTnI_{147-163}$ lies within the hydrophobic patch of open cNTnC. The peptide-induced conformational transition involves straightening of the B-helix at the kink

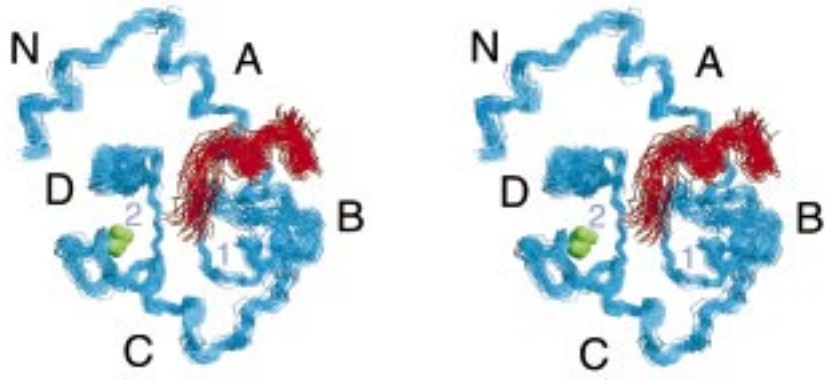

FIGURE 4: Stereoimage of the backbone superposition of the 40 structures of cNTnC·Ca^{2+}·$cTnI_{147-163}$. The backbone atoms (N, C_α, C′) of residues 5−85 of cNTnC are colored in light blue, the backbone atoms (N, C_α, C′) of residues 148−158 of $cTnI_{147-163}$ are colored in red, and Ca^{2+} ions are colored in green. The secondary structure of cNTnC in the complex is similar to cNTnC·apo and cNTnC·Ca^{2+} (*15*).

Table 3: Interhelical Angles for cNTnC and sNTnC

	A/B	B/C	C/D	A/D
cNTnC·apo (NMR)[a]	136 ± 3	118 ± 4	129 ± 5	113 ± 3
cNTnC·Ca^{2+} (NMR)[b]	132 ± 3	106 ± 4	117 ± 3	116 ± 3
cNTnC·Ca^{2+}·$cTnI_{147-163}$	102 ± 5	111 ± 7	96 ± 5	113 ± 3
sNTnC·apo (NMR)[c]	130 ± 3	126 ± 5	125 ± 4	111 ± 2
sNTnC·2Ca^{2+} (NMR)§[d]	90 ± 3	100 ± 6	69 ± 5	109 ± 3

[a] PDB accession code: 1SPY. [b] PDB accession code: 1AP4. [c] PDB accession code: 1TNP. [d] PDB accession code: 1TNQ.

(Glu-40) and conformational changes at Val-64. The opening of cNTnC·Ca^{2+} allows the peptide to bind in the hydrophobic pocket of cNTnC. The cNTnC·Ca^{2+}·$cTnI_{147-163}$ complex is stabilized by a large number of hydrophobic interactions which are summarized in Figure 5. In the structure of cNTnC·Ca^{2+}, the methyl groups of Ala-22, Ala-23, Ile-26, Val-44, Met-45, Met-47, Met-81, and Met-85 pack in the hydrophobic core of the protein. Upon binding $cTnI_{147-163}$, the distance between the backbone α-carbons of Met-81 (D-helix) and Asn-50 (BC-linker), for example, increases from 10 Å in cNTnC·Ca^{2+} to 18 Å in cNTnC·Ca^{2+}·$cTnI_{147-163}$. The peptide-induced increase in distance between the α-carbons of Met-81 and Asn-50 in cNTnC is compatible with a structural opening of cNTnC in which the BC structural unit swings away from the NAD unit, similar to that observed for the Ca^{2+}-induced opening of sNTnC (*10*, *11*).

The total "exposed" nonpolar accessible surface area using the Shrake definitions (*54*) for residues 5−84 of cNTnC, excluding the peptide, for the cNTnC·Ca^{2+}·$cTnI_{147-163}$ complex is 2879 ± 74 Å^2. This is an increase of 178 and 160 Å^2, compared to cNTnC·apo and cNTnC·Ca^{2+}, respectively (*15*). This increase in hydrophobic surface area for the complex is consistent with an open conformation for cNTnC and corresponds to the size of the hydrophobic patch that is involved in interactions with the peptide. For the analogous Ca^{2+}-induced opening of sNTnC, an increase of ∼500 Å^2 of hydrophobic surface is observed compared to sNTnC·apo (*10*, *11*), indicating that cNTnC in the cNTnC·Ca^{2+}·$cTnI_{147-163}$ complex is not as open as sNTnC·2Ca^{2+}.

DISCUSSION

Striated muscle contraction is triggered by Ca^{2+} binding to the regulatory domain of troponin-C. In the case of sTnC, Ca^{2+} binding induces a large conformational change with the exposure of a large hydrophobic patch, enabling the regulatory domain of sTnC to interact with its target protein, sTnI. For cNTnC, on the other hand, little structural change occurs upon Ca^{2+} binding, with a substantially reduced hydrophobic surface exposure compared to the skeletal isoform. This fundamental difference raises important questions regarding the mode of interaction between sTnC·sTnI and cTnC·cTnI. We have previously studied in detail the binding of a synthetic sTnI peptide ($sTnI_{115-131}$) binding to the regulatory domain of sNTnC and demonstrated that $sTnI_{115-131}$ binds in the hydrophobic pocket of sTnC and that the binding is kinetically competent for muscle contraction (*29*). In this study, we investigated the interaction between the corresponding cTnI peptide ($cTnI_{147-163}$) and the regulatory domain of cTnC. The results demonstrate that $cTnI_{147-163}$ binds cNTnC with 1:1 stoichiometry and that binding involves the hydrophobic core of the protein. Most importantly, $cTnI_{147-163}$ binds the open conformation of cNTnC, which is closed in the presence of Ca^{2+}. The structure of the complex is the first high-resolution structure of any cTnC·cTnI complex. It is clear from this work that the pathway involved in initiating skeletal and cardiac muscle contraction is similar, but the kinetics and thermodynamics of the pathway differ substantially for the two systems. That is, the end states for cNTnC·Ca^{2+}·$cTnI_{147-163}$ and sNTnC·2Ca^{2+}·$sTnI_{115-131}$ are similar, with both sNTnC and cNTnC binding their respective TnI peptides in an open conformation.

Comparison to Structural Change in sNTnC. The conformational change in cNTnC·Ca^{2+} that occurs upon binding $cTnI_{147-163}$ involves the BC unit moving away from the NAD unit. This peptide-induced conformational change in cNTnC·Ca^{2+} is similar to that observed for the apo to Ca^{2+}-saturated transition observed for sNTnC (*10*). The changes in interhelical angles induced by peptide binding are summarized in Table 3. In the apo-state of c- and sNTnC, the A/B and C/D interhelical angles are ∼130°. The A/B and C/D interhelical angles do not change much upon Ca^{2+} binding to cNTnC. Upon peptide binding, however, the A/B and C/D angles in cNTnC change to 102° and 96°, respectively. These values are comparable to the A/B and C/D angles of 90° and 69°, respectively, for sNTnC·2Ca^{2+}, indicating an opening for cNTnC. However, the larger A/B and C/D interhelical angles for cNTnC·Ca^{2+}·$cTnI_{147-163}$ indicate that the complex is slightly less open compared to sNTnC·2Ca^{2+}.

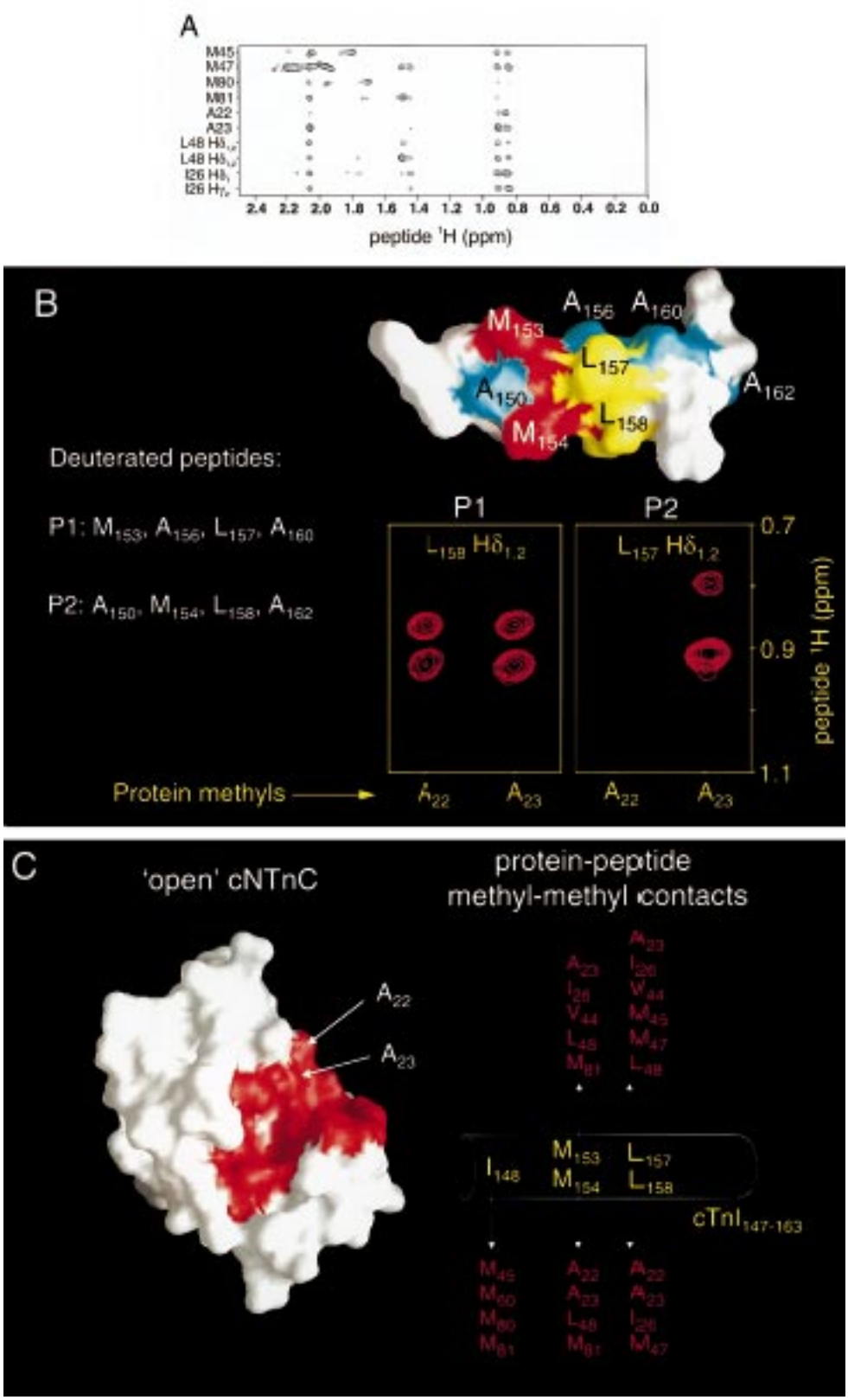

FIGURE 5: (A) Intermolecular methyl−methyl NOEs between unlabeled $cTnI_{147-163}$ and uniformly ^{13}C-labeled $cNTnC{\cdot}Ca^{2+}$. 3D ^{13}C F_1-edited, F_3-filtered NOESY−HSQC NMR spectra were collected at a $cTnI_{147-163}/cNTnC{\cdot}Ca^{2+}$ ratio of 3.5:1. (B) Strips taken from the 3D ^{13}C F_1-edited, F_3-filtered NOESY HSQC NMR spectra at the methyl ^1H-^{13}C chemical shifts of Ala-22 and Ala-23 of cNTnC. A GRASP (*56*) surface representation of a α-helical model of $cTnI_{147-163}$ is shown above panels P1 and P2. The panel P1 shows spectra acquired for the $cNTnC{\cdot}Ca^{2+}{\cdot}cTnI_{147-163}$ complex in which the side chain of Leu-157 of $cTnI_{147-163}$ was deuterated (peptide P1); thus both Ala-22 and Ala-23 show contacts to Leu-158 methyl protons. The panel labeled P2 shows spectra in which the side chain of Leu-158 of $cTnI_{147-163}$ was deuterated (peptide P2), and only Ala-23 shows contacts to Leu-157 methyls. Peptide P1 was deuterated at methyl groups of Met-153, Ala-156, Ala-160, and the side chain of Leu-157. Peptide P2 was deuterated at the methyl groups of Ala-150, Met-154, Ala-160, and the side chain of Leu-158. (C) Summary of protein−peptide residue pairs for which intermolecular methyl−methyl NOEs are observed between $cNTnC{\cdot}Ca^{2+}$ and $cTnI_{147-163}$. The molecular surface of a model of open cNTnC is shown, with residues which make contact with the peptide colored in red; residues Ala-22 and Ala-23 are indicated. Residues which make contact with peptide are buried in the hydrophobic core of $cNTnC{\cdot}Ca^{2+}$ (*15*), consistent with an open structure for cNTnC in the $cNTnC{\cdot}Ca^{2+}{\cdot}cTnI_{147-163}$ complex.

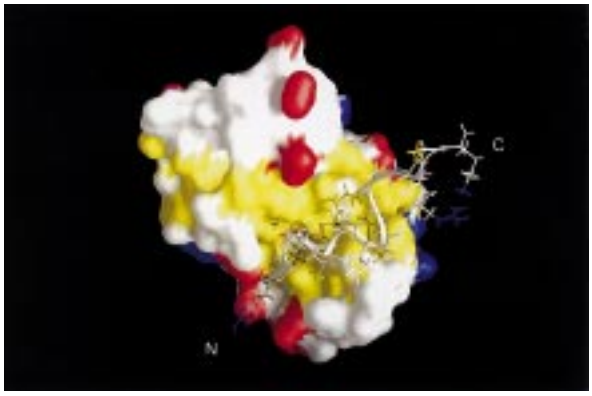

FIGURE 6: Molecular surface of cNTnC·Ca^{2+} (residues 5−84) in the cNTnC·Ca^{2+}·$cTnI_{147-163}$ complex. The structure of $cTnI_{147-163}$ is shown in the "rods" representation. The side chain atoms of hydrophobic residues (Ala, Leu, Ile, Met, Phe, Pro, Tyr, Val) are shown in yellow, negatively charged atoms are shown in red (Glu and Asp), positively charged atoms (Lys, Arg) are shown in blue, and all other atoms are colored in white. The figure was created with the program GRASP (*56*). The N- and C-terminal ends of the peptide are indicated.

Comparison to TnC-TnI Structural Models. The structure of the cNTnC·Ca^{2+}·$cTnI_{147-163}$ complex presented here is consistent with a model of cTnI and cTnC interacting in an antiparallel fashion, where the C-terminal region of cTnI binds to cNTnC (*3*). On the basis of the crystal structure of sTnC·$2Ca^{2+}$·$sTnI_{1-47}$ and previous structural data on the inhibitory region of sTnI (*16*), Maeda and co-workers (*17*) proposed a three-dimensional model of the sTnC·$4Ca^{2+}$·$sTnI_{96-127}$ complex. In this model, $sTnI_{111-127}$ adopts an α-helical conformation and interacts with the hydrophobic patch of sNTnC·$2Ca^{2+}$. The orientation of $sTnI_{111-127}$ bound to sNTnC·$2Ca^{2+}$ in the model is consistent with the orientation of bound $cTnI_{147-159}$ in the NMR structure of the cNTnC·Ca^{2+}·$cTnI_{147-163}$ complex presented here. Interestingly, in the model, the region of sTnI encompassing residues 128−131 does not interact with the hydrophobic patch of sNTnC, which is not surprising considering that this region (Ser-128, Lys-129, His-130, and Lys-131) is basic. One would expect that these residues extend outward away from the hydrophobic patch of sNTnC and perhaps interact with the hydrophilic surface residues of sNTnC or other thin filament proteins. Indeed, the NMR structure of cNTnC·Ca^{2+}·$cTnI_{147-163}$ shows that the C-terminal residues (160−163) of the peptide do not interact with cNTnC and remain disordered in the family of NMR structures for the complex, which suggests that this region of cTnI may play a similar structural role to that of $sTnI_{128-131}$. While the last four residues in $cTnI_{147-163}$ (Ala-160, Arg-161, Ala-162, and Lys-163) are not identical to those in the corresponding sTnI peptide, the basic residues Arg-161 and Lys-163 can be involved in electrostatic interactions at the rim of the hydrophobic patch in cNTnC.

In view of the four disordered C-terminal residues of cTnI, the choice of peptide used in this study may not be ideal for maximizing the interaction between the hydrophobic pocket of cNTnC and the hydrophobic face of $cTnI_{147-163}$. For example, $cTnI_{143-159}$ with additional N-terminal residues Leu-143, Arg-144, Arg-145, and Val-146 and C-terminal residues 160−163 removed could be used instead of $cTnI_{147-163}$. Modeling studies carried out in our laboratory suggest that it may be possible for this peptide to pass through the hydrophobic pocket of cNTnC in an α-helical conformation, similar to that for $cTnI_{147-163}$, but with Val-146 making hydrophobic contacts with the bottom of the hydrophobic pocket (residues on the C-helix of cNTnC), as opposed to $cTnI_{147-163}$, which has a turn at residue Ile-148 that allows the side chain of this residue to make hydrophobic contacts with the bottom of the hydrophobic pocket of cNTnC.

Relevance of cNTnC·Ca^{2+}·$cTnI_{147-163}$ Structure with Respect to Function. The structure of cNTnC·Ca^{2+}·$cTnI_{147-163}$ has important implications for the functional role of this region of cTnI encompassing residues 147−163. A recent study by Rarick et al. (*30*) has shown that the C-terminal region of cardiac TnI is essential for the Ca^{2+}-dependent regulation of cardiac myofilament activation. Their data suggest that the inhibitory region inhibits about 50% of the ATPase activity, while two other regions (residues 152−188, and 189−199 in mouse cTnI) contribute 25% each (*30*). Our finding that $cTnI_{147-163}$ interacts with the regulatory domain of cTnC in a Ca^{2+}-dependent fashion strongly supports the conclusions of Rarick et al. (*30*). The weak binding of $cTnI_{147-163}$ to cNTnC implies that cTnI binds cTnC in a fashion which allows the inhibitory protein to bind and release at a rapid rate. This property may be associated with the unique mechanism of heart muscle contraction.

Relevance to the Design of Pharmacological Agents for Treatment of Heart Failure. The troponin complex is a potential target for putative Ca^{2+}-sensitizing compounds designed to modify the Ca^{2+} dependence of cardiac muscle contraction. The ability to sensitize cardiac muscle to Ca^{2+} would have therapeutic potential for the treatment of Ca^{2+} desensitization that is associated with congestive heart failure due to acute myocardial infarction and associated ischemia (*55*). Ideally, the mechanism of sensitization would not involve altering Ca^{2+} transients in myocardial cells which would add the risk of toxic Ca^{2+} overload in the heart; rather it would increase the Ca^{2+}-binding affinity of the troponin complex. This can be accomplished by employing pharmaceutical agents which drive the following equilibrium to the right:

$$\text{cNTnC} + Ca^{2+} + \text{cTnI}_{147-163} \rightleftharpoons \text{cNTnC}\cdot Ca^{2+} + \text{cTnI}_{147-163} \rightleftharpoons \text{cNTnC}\cdot Ca^{2+}\cdot \text{cTnI}_{147-163}$$

One of the major structural changes in cNTnC·Ca^{2+} upon binding $cTnI_{147-163}$ is a movement of the B helix away from the A helix. Thus, the region of cNTnC located at the interface of the A and B helices is a likely target against which to design new and selective Ca^{2+}-sensitizing compounds.

Conclusions. This study was undertaken to investigate the interaction of cTnI with the regulatory domain of cTnC. A synthetic cTnI peptide, encompassing residues 147−163, was used to accomplish this task. The study demonstrates that the interaction between $cTnI_{147-163}$ and cNTnC is Ca^{2+}-dependent, which is consistent with the functional role of this region of cTnI. The three-dimensional solution structure of the complex demonstrates that, while cNTnC remains in the closed conformation in the Ca^{2+}-saturated state, $cTnI_{147-163}$ binds within the hydrophobic core of cNTnC in the presence of Ca^{2+}, thereby stabilizing cNTnC in an open conformation. The structure provides a framework for understanding the

details of the cTnC·cTnI interaction at the molecular level, an interaction which is fundamental in the Ca^{2+}-mediated regulation of cardiac muscle contraction.

ACKNOWLEDGMENT

We thank Murali Chandra and R. John Solaro for providing the cNTnC DNA construct; Lewis E. Kay for providing several pulse sequences; Stéphane Gagné for useful discussions; David Corson and Linda Saltibus for assistance with the protein purification; Gerry McQuaid for maintenance of the NMR spectrometers; Leigh Willard and Robert Boyko for computer expertise; and Brian Tripet and Ryan McKay for insightful discussions.

REFERENCES

1. Leavis, P. C., and Gergely, J. (1984) *CRC Crit. Rev. Biochem. 16*, 235−305.
2. Zot, A. S., and Potter, J. D. (1987) *Annu. Rev. Biophys. Biophys. Chem. 16*, 535−559.
3. Farah, C. S., and Reinach, F. C. (1995) *FASEB J. 9*, 755−767.
4. Tobacman, L. S. (1996) *Annu. Rev. Physiol. 58*, 447−481.
5. Putkey, J. A., Sweeney, H. L., and Campbell, S. T. (1989) *J. Biol. Chem. 264*, 12370−12378.
6. Sheng, Z., Strauss, W. L., Francois, J. M., and Potter, J. D. (1990) *J. Biol. Chem. 265*, 21554−21560.
7. Herzberg, O., and James, M. N. G. (1988) *J. Mol. Biol. 203*, 761−779.
8. Satyshur, K. A., Rao, S. T., Pyzalska, D., Drendal, W., Greaser, M., and Sundaralingham, M. (1988) *J. Biol. Chem. 263*, 1628−1647.
9. Slupsky, C. M., and Sykes, B. D. (1995) *Biochemistry 34*, 15953−15964.
10. Gagné, S. M., Tsuda, S., Li, M. X., Smillie, L. B., and Sykes, B. D. (1995) *Nat. Struct. Biol. 2*, 784−789.
11. Strynadka, N. C. J., Cherney, M., Sielecki, A. R., Li, M. X., Smillie, L. B., and James, M. N. G. (1997) *J. Mol. Biol. 273*, 238−255.
12. Houdusse, A., Love, M. L., Dominguez, R., Grabarek, Z., and Cohen, C. (1997) *Structure 5*, 1695−1711.
13. Herzberg, O., Moult, J., and James, M. N. G. (1986) *J. Biol. Chem. 261*, 2638−2644.
14. Sia, S. K., Li, M. X., Spyracopoulos, L., Gagné, S. M., Liu, W., Putkey, J. A., and Sykes, B. D. (1997) *J. Biol. Chem. 272*, 18216−18221.
15. Spyracopoulos, L., Li, M. X., Sia, S. K., Gagné, S. M., Chandra, M., Solaro, R. J., and Sykes, B. D. (1997) *Biochemistry 36*, 12138−12146.
16. Campbell, A. P., and Sykes, B. D. (1991) *J. Mol. Biol. 222*, 405−421.
17. Vassylyev, D. G., Takeda, S., Wakatsuki, S., Maeda, K., and Maeda, Y. (1998) *Proc. Natl. Acad. Sci. U.S.A. 95*, 4847−4852.
18. Olah, G. A., and Trewhella, J. (1994) *Biochemistry 33*, 12800−12806.
19. Stone, D. B., Timmins, P. A., Schneider, D. K., Kyrlova, I., Ramos, C. H. I., Reinach, F. C., and Mendelson, R. A. (1998) *J. Mol. Biol. 281*, 689−704.
20. Krudy, G. A., Kleerekoper, Q., Guo, X., Howarth, J. W., Solaro, R. J., and Rosevear, P. R. (1994) *J. Biol. Chem. 269*, 23731−23735.
21. Sheng, Z., Pan, B. S., Miller, T. E., and Potter, J. D. (1992) *J. Biol. Chem. 267*, 25407−25413.
22. Kobayashi, T., Grabarek, Z., Gergely, J., and Collins, J. H. (1995) *Biochemistry 34*, 10946−10952.
23. Farah, C. S., Miyamoto, C. A., Ramos, C. H. I., da Silva, A. C. R., Quaggio, R. B., Fujimori, K., Smillie, L. B., and Reinach, F. C. (1994) *J. Biol. Chem. 269*, 5230−5240.
24. Talbot, J. A., and Hodges, R. S. (1981) *J. Biol. Chem. 256*, 2798−2802.
25. Van Eyk, J. E., Thomas, L. T., Tripet, B. P., Wiesner, R. J., Pearlstone, J. R., Farah, C. S., Reinach, F. C., and Hodges, R. S. (1997) *J. Biol. Chem. 272*, 10529−10537.
26. Kobayashi, T., Tao, T., Grabarek, Z., Gergely, J., and Collins, J. H. (1991) *J. Biol. Chem. 266*, 13746−13751.
27. Pearlstone, J. R., Sykes, B. D., and Smillie, L. B. (1997) *Biochemistry 36*, 7601−7606.
28. Tripet, B. P., Van Eyk, J. E., and Hodges, R. S. (1997) *J. Mol. Biol. 271*, 728−750.
29. McKay, R. T., Tripet, B. P., Hodges, R. S., and Sykes, B. D. (1997) *J. Biol. Chem. 272*, 28494−28500.
30. Rarick, H. M., Tu, X. H., Solaro, R. J., and Martin, A. F. (1997) *J. Biol. Chem. 272*, 26887−26892.
31. Chandra, M., Dong, W. J., Pan, B. S., Cheung, H. C., and Solaro, R. J. (1997) *Biochemistry 36*, 13305−13311.
32. Gagné, S. M., Tsuda, S., Li, M. X., Chandra, M., Smillie, L. B., and Sykes, B. D. (1994) *Protein Sci. 3*, 1961−1974.
33. Li, M. X., Gagné, S. M., Tsuda, S., Kay, C. M., Smillie, L. B., and Sykes, B. D. (1995) *Biochemistry 34*, 8330−8340.
34. Golosinska, K., Pearlstone, J. R., Borgford, T., Oikawa, K., Kay, C. M., Carpenter, M. R., and Smillie, L. B. (1991) *J. Biol. Chem. 266*, 15797−15809.
35. Delaglio, F., Grzesiek, S., Vuister, G. W., Zhu, G., Pfeifer, J., and Bax, A. (1995) *J. Biomol. NMR 6*, 277−293.
36. Garrett, D. S., Powers, R., Gronenborn, A. M., and Clore, G. M. (1991) *J. Magn. Reson. 95*, 214−220.
37. Kay, L. E., Keifer, P., and Saarinen, T. (1992) *J. Am. Chem. Soc. 114*, 10663−10665.
38. Zhang, O., Kay, L. E., Olivier, J. P., and Forman-Kay, J. D. (1994) *J. Biomol. NMR 4*, 845−858.
39. Grzesiek, S., and Bax, A. (1992) *J. Am. Chem. Soc. 114*, 6291−6293.
40. Muhandiram, D. R., and Kay, L. E. (1994) *J. Magn. Reson., Ser. B 103*, 203−216.
41. Bax, A., Clore, G. M., and Gronenborn, A. M. (1990) *J. Magn. Reson. 88*, 425−431.
42. Kay, L. E., Xu, G. Y., Singer, A. U., Muhandiram, D. R., and Forman-Kay, J. D. (1993) *J. Magn. Reson., Ser. B 101*, 333−337.
43. Ogura, K., Terasawa, H., and Inagaki, F. (1996) *J. Biomol. NMR 8*, 492−498.
44. Pascal, S. M., Muhandiram, D. R., Yamazaki, T., Forman-Kay, J. D., and Kay, L. E. (1994) *J. Magn. Reson., Ser. B 103*, 197−201.
45. Gagné, S. M., Li, M. X., and Sykes, B. D. (1997) *Biochemistry 36*, 4386−4392.
46. Vuister, G. W., and Bax, A. (1993) *J. Am. Chem. Soc. 115*, 7772−7777.
47. Neri, D., Szyperski, T., Otting, G., Senn, H., and Wuthrich, K. (1989) *Biochemistry 28*, 7510−7516.
48. Zwahlen, C., Legault, P., Vincent, S. J. F., Greenblatt, J., Konrat, R., and Kay, L. E. (1997) *J. Am. Chem. Soc. 119*, 6711−6721.
49. Brünger, A. T. (1992) *X-PLOR Version 3.1 A system for X-ray Crystallography and NMR*, Yale University Press, New Haven, CT.
50. Li, M. X., Gagné, S. M., Spyracopoulos, L., Kloks, C. P. A. M., Audette, G., Chandra, M., Solaro, R. J., Smillie, L. B., and Sykes, B. D. (1997) *Biochemistry 36*, 12519−12525.
51. Kleerekoper, Q., Liu, W., Choi, D., and Putkey, J. A. (1998) *J. Biol. Chem. 273*, 8153−8160.
52. Wishart, D. S., and Sykes, B. D. (1994) *Methods Enzymol. 239*, 363−392.
53. Laskowski, R. A., MacArthur, M. W., Moss, D. S., and Thorton, J. M. (1993) *J. Appl. Crystallogr. 26*, 283−290.
54. Shrake, A., and Rupley, J. A. (1973) *J. Mol. Biol. 79*, 351.
55. Endoh, M. (1995) *Gen. Pharmacol. 26*, 1−31.
56. Nicholls, A. (1992) *GRASP: graphical representation and analysis of surface properties*, Columbia University, New York.

BI9901679